

**Lewis Acid-Base Pair Doping of p-Type Organic Semiconductors**

Journal:	<i>Journal of Materials Chemistry C</i>
Manuscript ID	TC-ART-02-2022-000605.R1
Article Type:	Paper
Date Submitted by the Author:	17-Mar-2022
Complete List of Authors:	Peterson, Kelly; University of California Santa Barbara, Materials Department Chabynyc, Michael; University of California Santa Barbara, Materials Department; Materials Department

# Lewis Acid-Base Pair Doping of *p*-Type Organic Semiconductors

Kelly A. Peterson,<sup>a</sup> Michael L. Chabinyc<sup>a</sup>

<sup>a</sup> *Materials Department, University of California, Santa Barbara, California 93106, USA*

## Abstract

Doping organic semiconductors is required to increase their electrical conductivity for uses in electronic and energy conversion devices. The limited number of commonly used *p*-type dopants suggests that new dopants or doping mechanisms could improve the efficiency of doping and provide new means for processing doped polymers. Drawing on Lewis acid-base pair chemistry, we combined Lewis acid dopant B(C<sub>6</sub>F<sub>5</sub>)<sub>3</sub> (BCF) with the weak Lewis base benzoyl peroxide (BPO). The detailed behavior of *p*-type doping of this Lewis acid-base pair in solution using model polymer poly(3-hexylthiophene) (P3HT) was examined. Solution <sup>19</sup>F-NMR spectra confirmed the formation of the expected counterion, as well as some side products. BCF:BPO was found to efficiently dope a range of semiconducting polymers with varying chemical structures demonstrating that the BCF:BPO combination has an effective electron affinity of at least 5.3 eV. In thin films of regioregular P3HT cast from the doped solutions, delocalized polarons formed due to the large counterions leading to a large polaron-counterion distance. At and above 0.2 eq. BCF:BPO doping, amorphous areas of the film became doped, disrupting the structural order of the films. Despite the change in structural order, thin films of P3HT doped with 0.2 eq. BCF:BPO had a conductivity of 25 S/cm. This study demonstrates the effectiveness of a two-component Lewis acid-base doping mechanism and suggests additional two-component Lewis acid-base chemistries should be explored.

## Introduction

Doping organic semiconductors is crucial to improving their electrical conductivity for applications in electronic and thermoelectric devices.<sup>1-3</sup> Organic semiconductors are typically doped with small molecules, but the number of highly effective, stable *p*-type dopants is relatively limited. Many *p*-type dopants have significant disadvantages including air or thermal instability, poor solubility in nonpolar solvents, and low efficiencies.<sup>2</sup> Another crucial aspect of doping semiconducting polymers is the interaction between doped polymers and molecular dopant counterions that frequently causes aggregation in solution and difficulty in processing homogeneous films.<sup>4,5</sup> Developing new dopants along with mechanistic understanding of their efficiencies will help to address these critical issues.

One promising *p*-type dopant is the Lewis acid tris(pentafluorophenyl)borane (BCF, B(C<sub>6</sub>F<sub>5</sub>)<sub>3</sub>). BCF has been found to dope organic semiconductors with a range of structures and comparable ionization energy (IE) ( $\approx 5$  eV) in solution, including poly(3-hexylthiophene) (P3HT),<sup>6-9</sup> poly[2,6-(4,4-bis(2-hexadecyl)-4Hcyclopenta[2,1-*b*;3,4-*b'*]dithiophene)-*alt*-4,7(2,1,3-benzothiadiazole)] (PCPDTBT),<sup>10</sup> and 2,2',7,7'-tetrakis[*N,N*-di(4-methoxyphenyl)amino]-9,9'-spirobifluorene (spiro-OMeTAD).<sup>11</sup> Electron spin resonance (ESR) spectroscopy confirmed that the reaction with BCF leads to formation of carriers with unpaired spin on the semiconductor.<sup>6,7,10,11</sup> The efficiency of formation of charge carriers with BCF is lower than the widely studied dopant 2,3,5,6-tetrafluoro-7,7',8,8'-tetracyanoquinodimethane (F<sub>4</sub>TCNQ) at equivalent molar ratios in solution.<sup>9,10</sup> However, in some cases the apparent charge carrier mobility in the doped material can be higher.<sup>10</sup>

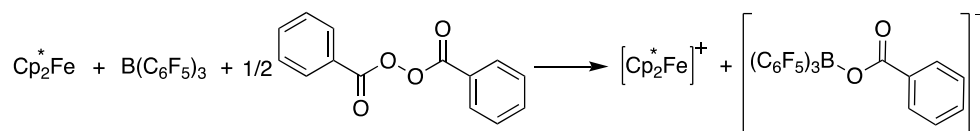
The mechanism of doping of organic semiconductors by BCF has been under wide investigation. Because BCF's electron affinity (EA) has been estimated at 3-3.5 eV,<sup>12,13</sup> simple integer charge transfer is an unlikely mechanism for generating charge carriers in organic semiconductors given that their IE is typically  $> 4.5$  eV. The BCF radical anion decomposes within

minutes<sup>14</sup> and reacts with solvents,<sup>12</sup> complicating efforts to detect it or to determine what role, if any, it might play in doping. Because BCF easily complexes with water to form a Brønsted acid,<sup>15</sup> an acid doping mechanism has been proposed to explain the observation of *p*-type doping.<sup>10</sup> The proposed mechanism for doping by strong acids is as follows: first, the acid protonates a polymer chain; next, the protonated polymer chain accepts an electron from a second (or other section of the initial) polymer chain; last, the now hydrogenated chain may undergo subsequent reactions. Supporting this mechanism, the addition of water was shown to increase BCF's doping efficiency with PCPDTBT.<sup>10</sup> Additional reaction steps in this mechanism have been proposed, including elimination of H<sub>2</sub> from hydrogenated polymer chains and formation of larger counterion complexes like [BCF(OH)(OH<sub>2</sub>)BCF]<sup>-</sup>. These additional reaction steps helped to rationalize the unfavorable energetics of the protonation reaction alone that were calculated using *ab initio* electronic structure methods.<sup>16</sup>

The chemical reactivity of BCF also presents challenges to understanding its interactions with organic semiconductors. In addition to acid doping by the complex BCF·H<sub>2</sub>O, BCF can participate in several other reactions that interfere with interpretation of its properties as a dopant. As a Lewis acid, BCF could form dative bonds with heteroatoms in organic semiconductors.<sup>17</sup> However, only a small group of polymers may be Lewis basic enough for complex formation, such as those with highly Lewis basic nitrogen atoms in their backbone.<sup>17-20</sup> One further complication of BCF's reactivity is that BCF and O<sub>2</sub> can act as a one-electron oxidant in the presence of a donor, forming the counterion [(C<sub>6</sub>F<sub>5</sub>)<sub>3</sub>B-O<sub>2</sub>-B(C<sub>6</sub>F<sub>5</sub>)<sub>3</sub>]<sup>-</sup>.<sup>21</sup> As these reactions suggest, the presence of differing amounts of water and oxygen along with varying solvents can make determination of a precise mechanism challenging.

Recent studies in one-electron oxidation reactions by Lewis acid-base pairs suggest a more energetically favorable way of utilizing BCF for one-electron oxidation. A Lewis acid and base pair may be sterically prevented from forming an adduct (a frustrated Lewis pair) or have a dissociative equilibrium.<sup>22</sup> These pairs can undergo reactions unlike conventional Lewis acid-base adducts. For example, when BCF is combined with a weak Lewis base, the formation of the Lewis pair (LP) can drive the single electron oxidation of decamethylferrocene.<sup>23</sup> In the proposed two-step mechanism for this reaction, BCF first oxidizes decamethylferrocene to form BCF radical anions. Then, BCF radical anions react with benzoyl peroxide (BPO), or another Lewis base, to form the counterion [PhC(O)O-B(C<sub>6</sub>F<sub>5</sub>)<sub>3</sub>]<sup>-</sup>, yielding the salt [Cp<sub>2</sub>\*Fe]<sup>+</sup>:[PhC(O)O-B(C<sub>6</sub>F<sub>5</sub>)<sub>3</sub>]<sup>-</sup>

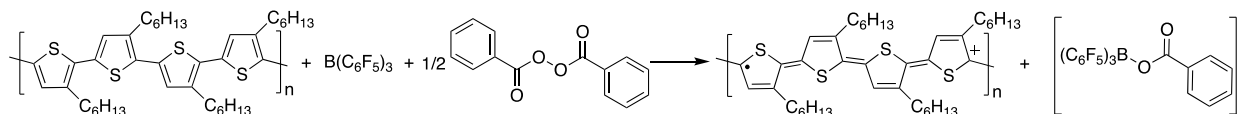
(Scheme 1).<sup>23</sup> Similar oxidation reactions have been demonstrated using oxygen<sup>21</sup> or quinones<sup>24</sup> as the weak Lewis base. The ability of Lewis acid-base pairs to carry out single electron transfer reactions suggests a route to increase the efficiency of BCF as a dopant for organic semiconductors.



**Scheme 1.** Oxidation of decamethylferrocene by  $\text{B}(\text{C}_6\text{F}_5)_3$  and benzoyl peroxide (BPO) reported by Reference 23<sup>23</sup>.

Here we show that rational design of doping reactions using LPs is a route to efficiently doping a wide range of semiconducting polymers. The Lewis base BPO increased the doping efficiency of BCF with several semiconducting polymers with differing backbone structures and ionization energies. Using regiorandom P3HT, we were able to confirm the expected product of the LP doping reaction. In the solid state, the LP mechanism led to high electrical conductivities and changes in the morphology of regioregular P3HT films.

## Results and discussion



**Scheme 2.** Proposed doping mechanism of P3HT with  $\text{B}(\text{C}_6\text{F}_5)_3$  and BPO.

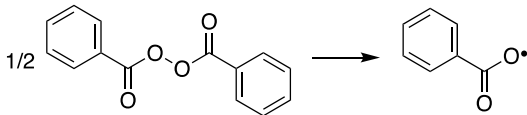
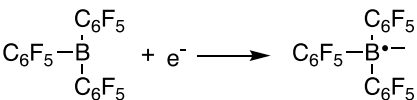
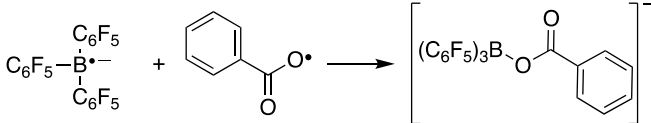
We explored the addition of BPO as a co-dopant for the reaction of BCF with P3HT as a model system (**Scheme 2**). BPO has been reported to form adducts with BCF in the absence of a donor, but reacts cleanly in the presence of  $[\text{Cp}_2^*\text{Fe}]$  to form a stable anion observed by NMR and by a single crystal structure.<sup>23</sup> While the mechanistic pathway is likely complex, we can split the proposed oxidation of a generic donor into four steps (**Table 1**). Among these reaction steps, the

ionization energy of the donor ( $IE_D$ ), electron affinity of BCF, and the homolytic bond dissociation energy of BPO are known or reasonably estimated. With the measured energies, we find the energy of formation of the known anion  $[\text{PhC(O)O-B(C}_6\text{F}_5)_3]^-$  ( $E_4$ ) can be related to the donor's ionization energy ( $IE_D$ ) by Equation (2). Given the reported facile reaction of  $[\text{Cp}^*\text{Fe}]$  with  $IE_D = 5.1$  eV,  $E_4$  must be  $-2.56$  eV or lower, a value comparable to the bond energy of a disulfide. This estimate suggests that the reaction should occur with donors with a range of values of  $IE_D$ .

$$E_1 + E_2 + E_3 + E_4 < 0 \#(1)$$

$$2.54 \text{ eV} - IE_D > E_4 \#(2)$$

**Table 1.** Fundamental processes and energetics of the overall oxidation reaction of a donor (D) with BCF and BPO.

	Reaction Step	Energy (eV)
$E_1$	$D \longrightarrow D^+ + e^-$	$IE_D$
$E_2$		$+0.76^a$
$E_3$		$-3.3^b$
$E_4$		$E_4$

<sup>a</sup> Activation energy of benzoyl peroxide decomposition measured at 146.0 kJ/mol by Reference 25.

<sup>b</sup> Standard reduction potential of  $\text{B(C}_6\text{F}_5)_3$  measured at  $-1.79$  V vs. ferrocene/ferrocenium in dichloromethane<sup>12</sup> and converted to  $-3.3$  eV per Reference 26.

We chose regioregular (RR-) and regiorandom P3HT (RRa-P3HT) as the model polymers to determine if Lewis pairs can act as dopants. P3HT has an ionization energy of 5 eV<sup>27</sup> that is similar to that of decamethylferrocene, and RRa-P3HT has an ionization energy that is slightly higher while being more soluble in polar solvents. The solubility is important because doped solutions of RR-P3HT are prone to forming polar aggregates that precipitate from non-polar solvents.<sup>4</sup> We annotate the amount of dopant used by equivalents (eq.) relative to the number of repeat units of P3HT in the solution. For solutions doped with BCF and BPO, BPO was always added in half of the molar amount of BCF as required by the expected doping reaction mechanism (Scheme 2); to simplify, the notation “BCF:BPO” represents this 1:0.5 ratio. We adapted our solvent choice in different experiments to accommodate the charged, doped polymers as much as possible, and to provide adequate signal in UV-Vis spectra.

We compared doping of P3HT by BCF and BCF:BPO by measuring the UV-Vis-NIR absorbance of the doped solutions. We note that, while we used BCF that was received dry and then prepared all solutions with anhydrous solvents in a N<sub>2</sub> glovebox, BCF can still scavenge even trace amounts of water in these environments.<sup>10</sup> As we doped RR-P3HT with increasing equivalents of BCF, the neutral P3HT peak at 450 nm decreased, and the two lower-energy features at 550-650 nm and 650-1000 nm increased in intensity (**Figure 1a**). The two peaks at 550-650 nm resemble the vibronic transitions associated with aggregated P3HT in solid-state films.<sup>28</sup> These peaks have been observed in BCF-doped RR-P3HT solution before and were found to be aggregates that could be filtered from the solution.<sup>8</sup> The feature at 650-1000 nm has been attributed to the absorbance of charged P3HT, i.e. polarons in P3HT.<sup>29</sup> The relatively flat shape of this feature has been connected to delocalized polarons within P3HT aggregates.<sup>8</sup> With addition of both BCF and BPO, the neutral P3HT peak at 450 nm was further bleached while the aggregation feature at 550-650 nm and the polaron absorbance at 650-1000 nm increased. Compared to solutions doped with the same amount of BCF, the BCF:BPO-doped solutions had greater bleaching of the neutral P3HT absorbance and greater increases in the lower-energy absorbances (Figure 1a & 1b). In contrast, when only BPO is added to the RR-P3HT solution, little change is observed in the spectrum. These spectra show that adding BPO increases the doping efficiency of BCF with RR-P3HT.

We examined the doping of RRa-P3HT with BCF:BPO in dichloromethane to help improve the solubility of the charged species relative to RR-P3HT. With increasing amounts of BCF:BPO, the absorbance of RRa-P3HT at 450 nm bleached, while lower-energy absorbances at the 550 nm shoulder, the 850 nm peak, and 1200-1600 nm tail increased (Figure 1c). These changes show that BCF:BPO can dope RRa-P3HT, despite its slightly larger ionization energy than RR-P3HT.<sup>27</sup> The absorbance shoulder at 550 nm suggests that RRa-P3HT began to aggregate in solution upon doping. Typically, the disorder in side chain position would prevent RRa-P3HT from crystallizing, but RRa-P3HT films have been observed to form ordered aggregates upon sequential F<sub>4</sub>TCNQ doping.<sup>30,31</sup> The shape of the polaron absorbance at 850 nm is consistent with that for the localized polarons of RRa-P3HT.<sup>9</sup> The polaron absorbance tail in the range 1200-1600 nm is also consistent with localized polarons because this peak redshifts with increasing polaron delocalization.<sup>9,32</sup> In our RR-P3HT spectra (**Figures 1a, 1b**), less of this absorbance tail is observed because the delocalized polaron absorbance would be expected at longer wavelengths than 1600 nm.

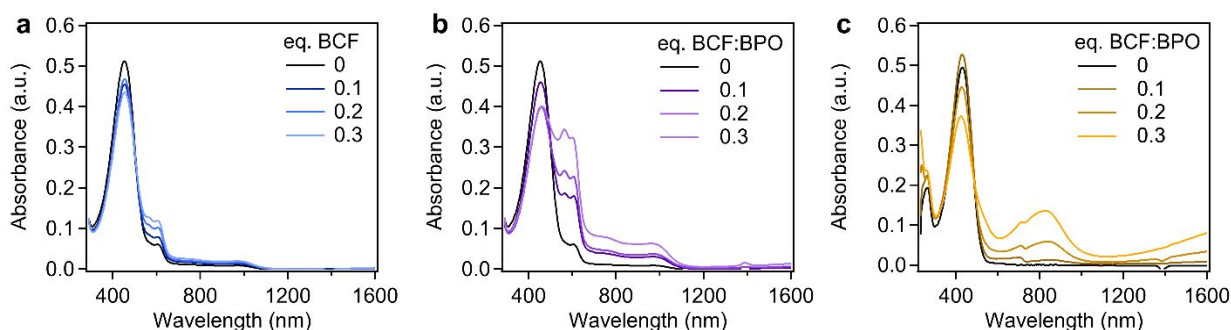


**Figure 1.** Solution UV-Vis spectra of (a) P3HT doped with BCF, (b) P3HT doped with BCF and BPO, and (c) RRa-P3HT doped with BCF and BPO. Solutions were measured at 0.0125 mg/mL of polymer in (a,b) chloroform or (c) dichloromethane. The small bumps in (c) spectra at 720 nm are due to spectrometer grating change.

**NMR Spectroscopy Confirms Reaction Pathway.** We used <sup>1</sup>H- and <sup>19</sup>F-NMR spectroscopy to confirm that the expected product [PhC(O)O-B(C<sub>6</sub>F<sub>5</sub>)<sub>3</sub>]<sup>-</sup> could be produced in a reaction of a semiconducting polymer with BCF and BPO. We chose RRa-P3HT because the signal from its aromatic protons is upfield from the peaks of BPO and it can dissolve in CD<sub>2</sub>Cl<sub>2</sub> for easier



comparison with the known compound with  $[\text{Cp}_2^*\text{Fe}]$  (**Scheme 1**). Because dichloromethane has been shown to react with the BCF radical anion,<sup>12</sup> we also expected to observe side products, alongside other potential reactions between BCF and residual water or oxygen. The paramagnetic species and electrostatic interactions in our system also interfered with interpretation of these spectra; the  $[\text{PhC}(\text{O})\text{O}-\text{B}(\text{C}_6\text{F}_5)_3]$  counterion is diamagnetic, while doped RRa-P3HT chains are paramagnetic. The complete NMR spectra are presented in the **Supporting Information (Figures S3-18)**, and we discuss the most relevant spectral regions of the precursors and doped solutions here.

To compare the products of the RRa-P3HT, BCF, and BPO reaction to the known reaction with  $[\text{Cp}_2^*\text{Fe}]$ , we synthesized the  $[\text{Cp}_2^*\text{Fe}]^+:[\text{PhC}(\text{O})\text{O}-\text{B}(\text{C}_6\text{F}_5)_3]^-$  salt following the reported procedure.<sup>23</sup> The  $^{19}\text{F}$ -NMR signals of  $[\text{PhC}(\text{O})\text{O}-\text{B}(\text{C}_6\text{F}_5)_3]^-$  (**Figure 2**) were at -135 (d, *o*- $\text{C}_6\text{F}_5$ ), -163.4 (t, *p*- $\text{C}_6\text{F}_5$ ), and -167.6 ppm (t, *m*- $\text{C}_6\text{F}_5$ ), consistent with the reported values.<sup>23</sup> The second set of signals is consistent with wet BCF<sup>15</sup> that likely formed when excess BCF starting material in the product was exposed to air. In the BCF:BPO-doped RRa-P3HT spectrum, peaks for  $[\text{PhC}(\text{O})\text{O}-\text{B}(\text{C}_6\text{F}_5)_3]^-$  appear shifted downfield by 0.3-0.4 ppm from the peaks of the  $[\text{Cp}_2^*\text{Fe}]^+$  complex at -134.7, -163.1, and -167.2 ppm (**Figure 2**, red bands). Because NMR signals are highly sensitive to the electronic environment, we expected shifts from differences in electronic localization or dielectric environment between samples.

The  $^{19}\text{F}$ -NMR spectrum for RRa-P3HT + 0.1 eq. BCF:BPO also has signals for several other species, indicating the presence of side products. The most noticeable is a doublet of multiplets at -139 ppm and complex multiplets at -154.5 and -162.7 ppm (blue bands) with a roughly 2:1:2 area ratio. While these peaks appear taller than the  $[\text{PhC}(\text{O})\text{O}-\text{B}(\text{C}_6\text{F}_5)_3]^-$  peaks in **Figure 2**, the area ratio between the  $[\text{PhC}(\text{O})\text{O}-\text{B}(\text{C}_6\text{F}_5)_3]$  peaks and this product is 3:2. These peaks appear in many spectra, including RRa-P3HT + 0.3 eq. BCF and BCF:BPO, suggesting a common impurity of BCF not caused by side reactions with RRa-P3HT or BPO. Ruling those reactions out leaves reactions between BCF radical anions and the solvent,  $\text{CD}_2\text{Cl}_2$ , as the more likely cause. Five products of reduced BCF and dichloromethane (DCM) have been previously identified,<sup>12</sup> but the *ortho*-F signals for these products are all 4-7 ppm downfield of our product's doublet signal. The  $^1\text{H}$ -NMR also show evidence of the product anion, along with other features from side products that were difficult to assign definitively (**See Supporting Information Figure S3**). The assigned BCF- $\text{CD}_2\text{Cl}_2$  peaks (blue bands) did not appear in the spectrum of

$[\text{Cp}_2^*\text{Fe}]^+:[\text{PhC}(\text{O})\text{O}-\text{B}(\text{C}_6\text{F}_5)_3]^-$  (**Figure 2**), but unlike the reaction mixtures prepared directly in  $\text{CD}_2\text{Cl}_2$ , the salt was precipitated and washed with pentane before measurement. Given these data, the side products here may differ from the previously identified products of the reactions of  $\text{CH}_2\text{Cl}_2$  with BCF alone, or the signal may be shifted due to the local environment. Overall, the NMR spectra show formation of the proposed product, along with side products, including those formed between BCF and solvent, thereby demonstrating the complexity of defining all of the reaction pathways of BCF with semiconducting polymers and the importance of solvent choice.

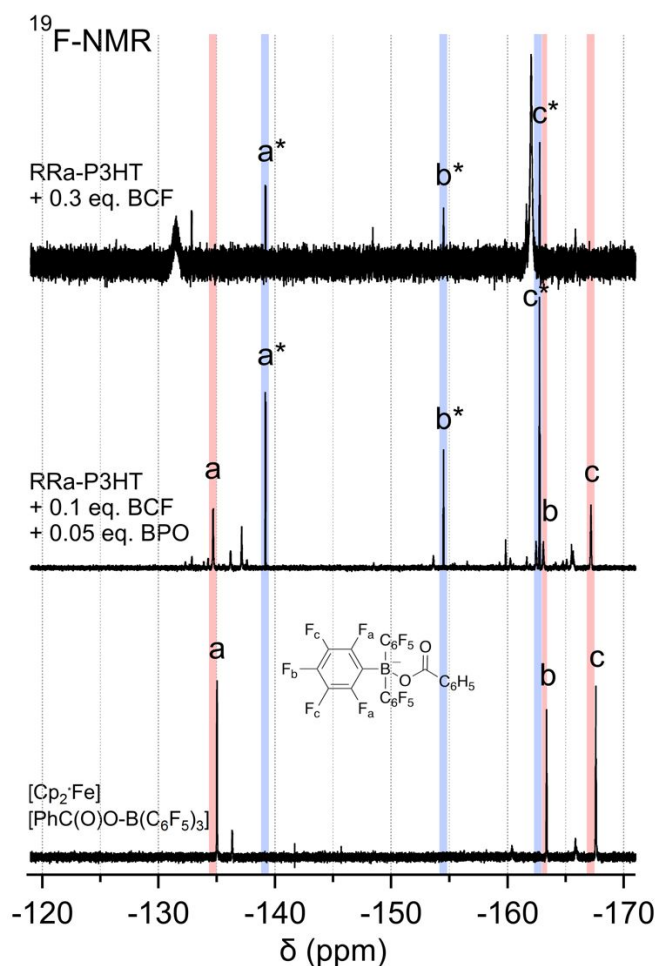


**Figure 2.**  $^{19}\text{F}$ -NMR spectra of  $[\text{Cp}_2^*\text{Fe}]^+:[\text{PhC}(\text{O})\text{O}-\text{B}(\text{C}_6\text{F}_5)_3]^-$  (bottom) and BCF:BPO- (middle) and BCF-doped RRa-P3HT (top) solutions in  $\text{CD}_2\text{Cl}_2$ . Red bands assigned to  $[\text{PhC}(\text{O})\text{O}-\text{B}(\text{C}_6\text{F}_5)_3]^-$  product with *ortho*- (a), *para*- (b), and *meta*- (c) F atoms labeled. Blue bands indicate common side reaction product, with a\*, b\*, and c\* labeling the likely *ortho*-, *para*-, and *meta*-F atoms, respectively.

**Doping by Lewis Pairs Occurs Across Semiconducting Polymers.** We examined doping of several other conjugated polymers with a range of backbone structures and ionization energies using BCF:BPO. We note that the BCF used for these experiments was found to have a higher water content than those in **Figure 1** and we make the distinction by noting the dopant as  $\text{BCF}\cdot(\text{H}_2\text{O})_x$ .  $^{19}\text{F}$ -NMR peaks of this  $\text{BCF}\cdot(\text{H}_2\text{O})_x$  in  $\text{CD}_2\text{Cl}_2$  shifted further upfield than those of  $\text{BCF}\cdot(\text{H}_2\text{O})$ ,<sup>15</sup> indicating that our  $\text{BCF}\cdot(\text{H}_2\text{O})_x$  contained more than 1 eq. of water ( $x > 1$ ) (see **SI Figure S19**). Because water atoms are loosely bound to BCF and the BCF:BPO reaction is expected to be more energetically favorable, we did not expect the presence of water to inhibit the formation of  $[\text{PhC}(\text{O})\text{O}-\text{B}(\text{C}_6\text{F}_5)_3]^-$ . Furthermore, we expect that these results represent more typical conditions with BCF where it is difficult to fully exclude water. First, we examined the reaction of  $\text{BCF}\cdot(\text{H}_2\text{O})_x$ :BPO and  $\text{BCF}\cdot(\text{H}_2\text{O})_x$  with the donor-acceptor co-polymer indacenodithiophene-*co*-benzothiadiazole with ethylhexyl side chains ( $\text{C}_2\text{C}_6$ -IDTBT) in chlorobenzene.  $\text{C}_2\text{C}_6$ -IDTBT has an ionization energy of 5.3 eV,<sup>33</sup> and its benzothiadiazole unit provides the potential ability to complex with BCF. Little doping was observed from  $\text{BCF}\cdot(\text{H}_2\text{O})_x$  alone in chlorobenzene solution (**Figure 3a**). When  $\text{BCF}\cdot(\text{H}_2\text{O})_x$ :BPO was used for doping, the main absorbances at  $\sim 400$  nm and  $\sim 650$  nm were bleached while new peaks appeared at  $\sim 1050$  and 1600 nm. The spectrum of doped IDTBT was consistent with bleaching of the main transition and an increase in sub-gap absorption peaked at 1100 nm in charge accumulation spectroscopy of an IDTBT field effect transistor.<sup>34</sup> These changes again indicate that  $\text{BCF}\cdot(\text{H}_2\text{O})_x$ :BPO was a more efficient dopant for IDTBT than  $\text{BCF}\cdot(\text{H}_2\text{O})_x$ .

To examine doping of a polymer without Lewis basic heteroatoms in the backbone, we chose poly[2-methoxy-5-(2-ethylhexyloxy)-1,4-phenylenevinylene] (MEH-PPV). MEH-PPV has a comparable ionization energy (5.3 eV) to IDTBT.<sup>35</sup> After mixing MEH-PPV with  $\text{BCF}\cdot(\text{H}_2\text{O})_x$  in chlorobenzene solution, only a weak new absorbance was observed  $\sim 850$  nm (**Figure 3b**). When MEH-PPV was mixed with  $\text{BCF}\cdot(\text{H}_2\text{O})_x$  and BPO (Fig. 3b), the polymer absorbance at 500 nm was bleached and blue-shifted, while new absorbances appeared at  $\sim 850$  and 1600 nm. These changes match those observed for doping of MEH-PPV with the oxidant magic blue.<sup>35</sup> Again,  $\text{BCF}\cdot(\text{H}_2\text{O})_x$ :BPO is a more efficient dopant than  $\text{BCF}\cdot(\text{H}_2\text{O})_x$ .

To test the limits of doping, we choose polyfluorene, PFO, which has a large ionization energy at 5.8 eV<sup>36</sup> and no heteroatoms. Upon addition of  $\text{BCF}\cdot(\text{H}_2\text{O})_x$  and  $\text{BCF}\cdot(\text{H}_2\text{O})_x$ :BPO in chlorobenzene solution (**Figure 3c**), no changes in the spectra were observed. This lack of an

observed doping reaction provides a bound for the reaction  $E_4$  to be between -2.8 and -3.3 eV and that the net reaction of BCF:BPO can oxidize donors with  $IE_D$  less than 5.8 eV.

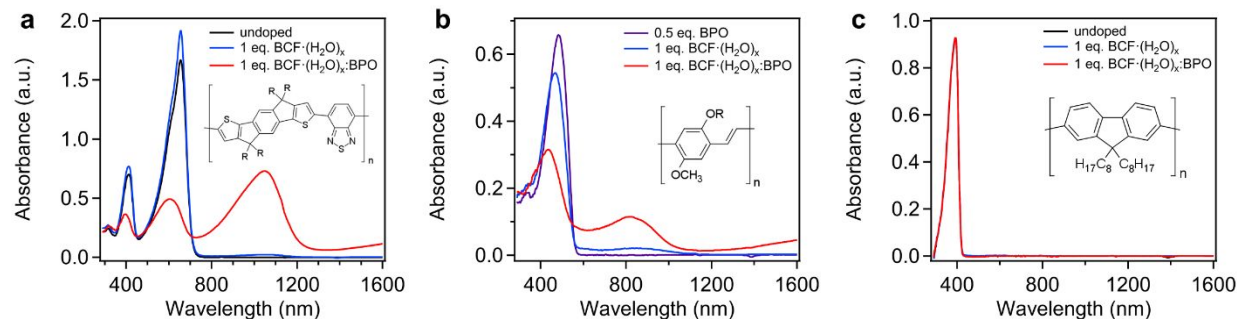


**Figure 3.** Solution UV-Vis spectra of (a) MEH-PPV, (b) IDTBT, and (c) PFO mixed with BCF·(H<sub>2</sub>O)<sub>x</sub> or BCF·(H<sub>2</sub>O)<sub>x</sub>:BPO at 0.02 mg/mL of polymer in chlorobenzene. R = 2-ethylhexyl.

**Microstructure of Doped Films Becomes More Disordered with Increasing Dopant.** After confirming that BCF:BPO is an effective dopant for a range of semiconducting polymers in solution, we examined how this doping process affects solid state properties using RR-P3HT. The relatively large [PhC(O)O-B(C<sub>6</sub>F<sub>5</sub>)<sub>3</sub>]<sup>-</sup> counterion ( $\approx 1.2$  nm long) could disrupt ordering of semiconducting polymers in the solid state. We chose to focus on RR-P3HT for comparison to studies of doping with BCF alone and other large dopants. In the neat RR-P3HT film, we observed the expected P3HT spectrum with vibronic features indicative of aggregation into crystallites (**Figure 4a**).<sup>28,37</sup> As the dopant ratio in the solutions increased, the absorbance of the neutral P3HT peak decreased in the films, while two features, attributed to the polarons and labeled P1 and P2, increased. A theoretical model based on aggregates of polymer chains and experiments have shown that the shape of P1 changes with the delocalization of the polaron and distance of the counter-anion to the polaron.<sup>32,38,39</sup> As polaron delocalization increases, P1a (0.1 eV) is predicted to redshift and increase, while P1b (0.2-1 eV) also redshifts with more sensitivity to the polaron-anion distance.<sup>32</sup> In a two-polaron model, P1 can redshift further, matching electrochemical doping experiments,<sup>40</sup> but without hole-hole repulsions, bipolarons can localize and blueshift P1.<sup>41</sup> At 1 eq. BCF:BPO doping, the P3HT peak was completely bleached. The strongest absorbance is centered at 0.6 eV while P1a and P2 decrease below the 0.2 eq. BCF:BPO spectrum. The decreases in P1a and P2 suggest that the amount of polarons in the film is decreasing. DFT calculations of oxidized poly(ethylenedioxythiophene) chains suggest that, below 33% oxidation, the two polaron

transitions will shift towards each other due to mixed valency along the chain. At 33% oxidation, the chain is a closed-shell singlet with one optical transition.<sup>42</sup> Based on these calculations, our 1 eq. BCF:BPO-doped film could contain a mix of intermediate open-shell P3HT oxidation states with interacting polarons, such as paired polarons. Similar spectra have been observed in intermediate electrochemically doped P3HT<sup>40,43</sup> and polythiophene,<sup>44</sup> as well as FeCl<sub>3</sub>-doped P3HT.<sup>45</sup>

In our 0.05 – 0.3 eq. BCF:BPO-doped films, P1 and P2 can provide information about the morphology of the films and the delocalization of the polarons. In all of our film spectra, the locations of P1a and P1b, as well as their relative ratios, were consistent with highly delocalized polarons (**Figure 4b**). The peak of P1b is at 0.34-0.36 eV. This location matches that seen in P3HT doped with dodecaborane dopants with diameters  $\approx 2$  nm.<sup>46</sup> We fit P1 in our data with several Gaussian functions to calculate the area of the peaks (**Supporting Information Figure S27**). We found that the area on the high-energy side of P1b increased disproportionately to the rest of P1 with doping. A shoulder in P1 at 0.8-1 eV has been observed in F<sub>4</sub>TCNQ-doped P3HT and was attributed to localized polarons that are closer to the F<sub>4</sub>TCNQ<sup>-</sup> counterion.<sup>47</sup> Alternately, a blueshift in P1 could be caused by higher open-shell oxidation states, as in the 1 eq. BCF:BPO-doped spectrum.

The shape of P2 has been connected to the degree of aggregation in P3HT solutions. In our BCF:BPO-doped films (**Figure 4a**), P2 in the two lower doped films is a relatively flat shoulder. In the two more highly doped films, an absorbance peak at 1.5 eV is the predominant feature in P2. This trend of P2 changing shape with increasing doping has been observed before in FeCl<sub>3</sub>- and NOPF<sub>6</sub>-doped P3HT films.<sup>45,48</sup> In experiments with BCF-doped P3HT solutions, the flat shoulder was associated with aggregates that can be filtered out of the solution.<sup>8</sup> Comparisons of doped regioregular and RRa-P3HT solutions showed that regioregular P3HT had a relatively flat P2, while RRa-P3HT's P2 had a peak centered at 1.5 eV.<sup>9</sup> Based on these findings, the change in shape of P2 in our films (**Figure 4a**) at the higher doping levels could indicate that more amorphous areas of the films were doped. With the high-energy increase in P1b, the shape changes in P1b and P2 likely indicate that, as doping increases, polarons increasingly form in the amorphous areas of the film.

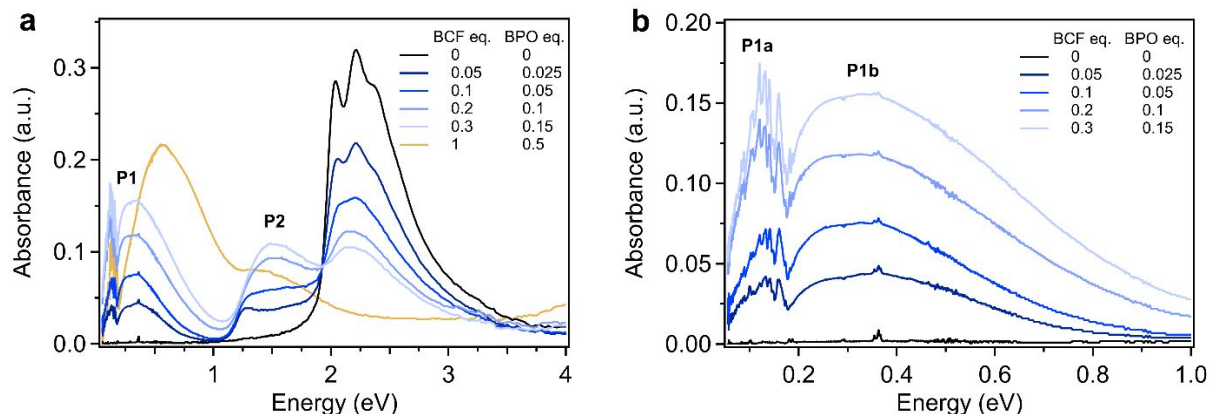


**Figure 4.** (a) Full and (b) IR region of combined film UV-Vis and FTIR spectra of BCF:BPO-doped RR-P3HT films cast from 9:1 v/v chloroform:acetonitrile solution on KBr plates.

We carried out grazing incidence wide-angle X-ray scattering (GIWAXS) to determine how the large counterion from BCF:BPO doping affected the microstructure of RR-P3HT relative to BCF alone. The neat RR-P3HT films (**Figure 5a**) had an alkyl stacking distance of 16.2 Å and a  $\pi$ - $\pi$  stacking distance of 3.88 Å in agreement with literature,<sup>49</sup> and the crystallites had a dominantly edge-on texture. In doped films with BCF or BCF:BPO, the alkyl stacking distance increased, and the  $\pi$ - $\pi$  stacking distance decreased (**Table 2, Supporting Information Figures S22-25**). These changes in stacking distances are consistent with dopants being incorporated into P3HT crystallites between the alkyl chains.<sup>49</sup> In P3HT films, vapor doping with F<sub>4</sub>TCNQ can increase alkyl stacking up to 18 Å,<sup>49</sup> while sequential doping with dodecaborane-based dopants increased alkyl stacking up to 31 Å.<sup>46</sup> In the film cast from P3HT solution doped with 0.1 eq. BCF:BPO (**Figure 5b**), the edge-on crystalline texture is still present with alkyl stacking of 19.0 Å and  $\pi$ - $\pi$  stacking of 3.80 Å. This increase in alkyl stacking was larger than in the equivalent 0.1 eq. BCF-doped film (**Table 2**). The larger [PhC(O)O-B(C<sub>6</sub>F<sub>5</sub>)<sub>3</sub>]<sup>-</sup> counterion, or increased incorporation of the counterion from the higher doping efficiency of BCF:BPO, could cause this larger increase in alkyl stacking. At the higher doping level of 0.2 eq. BCF:BPO, greater changes were observed (**Figure 5c**) with a decrease in scattering intensity indicating a decrease in structural ordering. The stacking distances could still be extracted, with alkyl stacking at 19.5 Å and  $\pi$ - $\pi$  stacking at 3.67 Å. In a previous study of BCF-doped P3HT, films also became increasingly disordered with doping, and alkyl stacking distances up to 19.2 Å were observed at doping levels of 40%.<sup>7</sup> Our 0.2 eq. BCF:BPO-doped film had additional scattering at  $q_z = 0.48 \text{ \AA}^{-1}$  (13 Å)

between the first two alkyl stacking peaks. It is possible that this feature is due to scattering between counterions and polymer chains or due to a second phase, as suggested for in dodecaborane-doped P3HT,<sup>46</sup> but with one feature it is not possible to make a definitive assignment of the structure. Overall, the scattering changes significantly between the 0.1 eq. and 0.2 eq. levels of BCF:BPO, correlating with the change in the UV-Vis spectra at 1.5 eV that is associated with more localized polarons (**Figure 4**). Together, these changes indicate that the increases in disorder and in localized polarons with doping are connected.

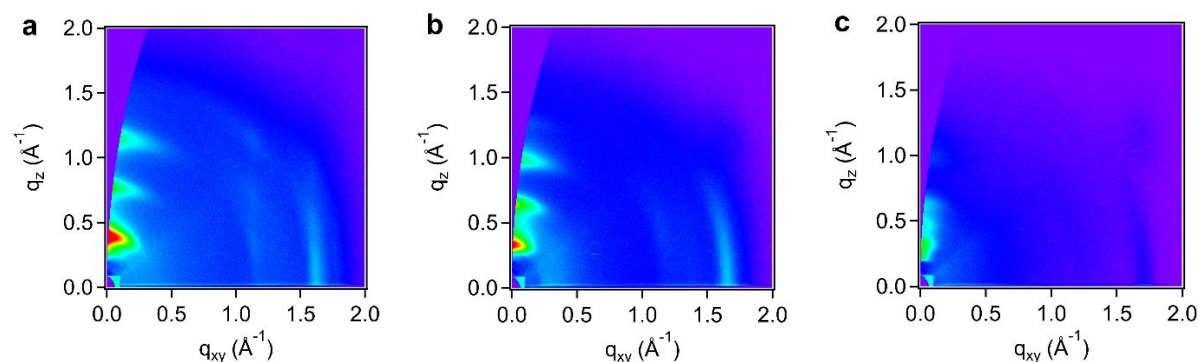


**Figure 5.** Grazing incidence wide-angle X-ray scattering images of (a) undoped RR-P3HT and RR-P3HT films doped with (b) 0.1 eq. BCF:BPO and (c) 0.2 eq. BCF:BPO.

**Table 2.** Alkyl and  $\pi$ - $\pi$  stacking distances of BCF- and BCF:BPO-doped RR-P3HT films extracted from GIWAXS scattering images.

	Alkyl Stacking (Å)	$\pi$ - $\pi$ Stacking (Å)		Alkyl Stacking (Å)	$\pi$ - $\pi$ Stacking (Å)
neat film	16.2	3.88			
0.05 eq. BCF	16.7	3.85	0.05 eq. BCF:BPO	17.5	3.79
0.1 eq. BCF	17.0	3.70	0.1 eq. BCF:BPO	19.0	3.80
0.2 eq. BCF	18.3	3.78	0.2 eq. BCF:BPO	19.5	3.67
0.3 eq. BCF	18.8	3.75	0.3 eq. BCF:BPO	18.5	3.75

***Co-doping with BCF:BPO leads to high conductivity films.*** We measured the in-plane conductivity of BCF- and BCF:BPO-doped RR-P3HT films using the four-point probe method (**Figure 6**). At and above 0.1 eq. BCF, doping with BCF:BPO increased the conductivity of the films over those doped with BCF alone. The maximum conductivity measured was  $25 \pm 6$  S/cm for the film doped with 0.2 eq. BCF:BPO. While the more disordered morphology measured in **Figure 5c** could be expected to be detrimental for hole transport, we measured the highest conductivities for the 0.2 eq. BCF:BPO- and 0.3 eq. BCF:BPO-doped films. The increase in carrier concentration at these doping levels may offset the disruption in order, or the disordered morphology of **Figure 5c** may be deceptively beneficial for charge transport. For example, formation of localized polarons at higher doping levels could disrupt aggregate formation while still providing intercrystallite transport pathways.

The electrical conductivities from solution-based doping with BCF:BPO compare favorably with other dopants and processing routes. One of the highest reported values of conductivity for RR-P3HT doped with BCF is 33 S/cm; this value was achieved with 120% BCF, which implies that the amount of BCF and polymer were nearly equivalent in the solid.<sup>7</sup> The higher efficiency of doping with BCF:BPO leads to higher conductivity at lower concentration of dopant. RR-P3HT solution-doped with F<sub>4</sub>TCNQ has been reported to have conductivity up to 8.0 S/cm at 17 mol% F<sub>4</sub>TCNQ,<sup>50</sup> with conductivity observed to decrease at F<sub>4</sub>TCNQ mole fractions above 0.17.<sup>51</sup> The larger effective electron affinity of BCF:BPO relative to F<sub>4</sub>TCNQ can lead to a higher carrier concentration, while the higher solubility of BCF:BPO in nonpolar solvents can improve processability. A relatively large dopant (~ 2 nm) based on dodecaborane yielded RR-P3HT films with conductivity up to 12.8 S/cm using sequential doping.<sup>52</sup> Despite the large size of the counterion here, the electrical conductivity is comparable, suggesting that large counterions can still be effective dopants if they maintain processability of the polymer.



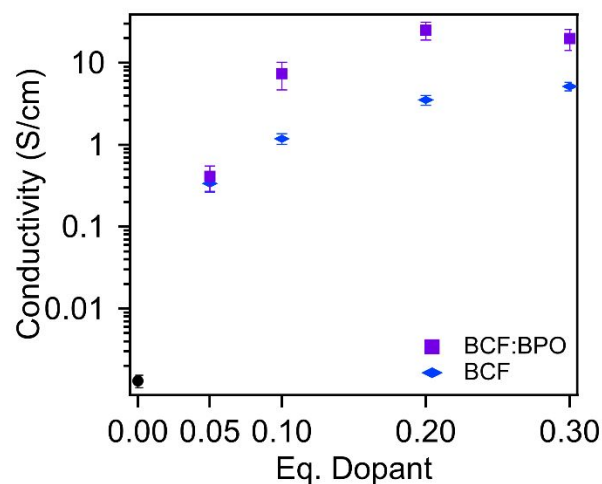


**Figure 6.** Conductivity of BCF- (blue diamonds) and BCF:BPO-doped (purple squares) RR-P3HT films cast from doped solution. Error bars were calculated by error propagation of the standard deviation of three measurements on each film and the film roughness.

## Conclusion

We have demonstrated that single electron transfer from a Lewis acid-base pair, BCF:BPO, is a route to increase the efficiency of doping over a Lewis acid, BCF, alone. The BCF:BPO combination can dope semiconducting polymers with various backbone structures up to ionization energies of at least 5.3 eV. Using  $^{19}\text{F}$ -NMR spectroscopy, we found the expected counterion product,  $[\text{PhC}(\text{O})\text{O}-\text{B}(\text{C}_6\text{F}_5)_3]^-$ . Despite the relatively large size of the counterion, films of P3HT doped with BCF:BPO had high electrical conductivities of  $25 \pm 6$  S/cm with 0.2 eq. of dopant. Optical spectroscopy showed that the films have highly delocalized polarons with the proportion of more localized polarons increasing with increasing doping. These localized polarons suggest that, above some threshold, polarons increasingly form in amorphous areas of the films with increasing disruption of the crystallite structure. Given that the P3HT film conductivity is higher than that with  $\text{F}_4\text{TCNQ}$  or BCF doping from solution, these localized polarons and disruption in ordering do not seem to be detrimental to electrical transport.

Our results show that LPs can be used to *p*-type dope semiconducting polymers and that the addition of BPO can improve the doping efficiency and effective electron affinity over BCF alone. The energetic stabilization of B-O bond formation in the proposed reaction mechanism drives the doping reaction, in contrast to the unclear doping mechanism of BCF alone. The many

Lewis bases that have already been demonstrated to stabilize one-electron oxidation with BCF offer further ways to adjust the effective electron affinity and counterion size during doping.<sup>21,23,24,53</sup> Similar Lewis acids, such as  $\text{Al}(\text{C}_6\text{F}_5)_3$  and  $\text{Zn}(\text{C}_6\text{F}_5)_3$ , may be useful in doping, as well.<sup>23,54,55</sup> Like  $\text{F}_4\text{TCNQ}$ , BCF can be sublimated, so vapor infiltration of BCF may offer an additional route to optimize processing of LP-doped films. With this new LP route to oxidizing polymers, we anticipate that more dopants with the desired properties for electronic and thermoelectric devices may be found.

## Author contributions

The manuscript was written through contributions of all authors. All authors have given approval to the final version of the manuscript.

## Conflicts of interest

There are no conflicts of interest to declare.

## Acknowledgements

This work was supported by the National Science Foundation (NSF) under DMR 1808622. Portions of this work were carried out at the MRL Shared Experimental Facilities, supported by the NSF MRSEC program under award no. DMR 1720256. Use of the Stanford Synchrotron Radiation Lightsource, SLAC National Accelerator Laboratory, is supported by the U.S. Department of Energy, Office of Science, Office of Basic Energy Sciences under Contract No. DE-AC02-76SF00515. Use was made of computational facilities purchased with funds from the National Science Foundation (CNS-1725797) and administered by the Center for Scientific Computing (CSC). The CSC is supported by the California NanoSystems Institute (CNSI) and the MRSEC (NSF DMR 1720256) at UC Santa Barbara. We thank Prof. Iain McCulloch (Oxford University) for the sample of IDTBT. We also acknowledge helpful discussions and assistance at UCSB from Dr. Amir Mazaheripour, Saejin Oh, and Zhifang Du.

## References

- 1 A. D. Scaccabarozzi, A. Basu, F. Aniés, J. Liu, O. Zapata-Arteaga, R. Warren, Y. Firdaus, M. I. Nugraha, Y. Lin, M. Campoy-Quiles, N. Koch, C. Müller, L. Tsetseris, M. Heeney and T. D. Anthopoulos, *Chem. Rev.*, 2021 DOI:10.1021/acs.chemrev.1c00581.
- 2 I. E. Jacobs and A. J. Moulé, *Adv. Mater.*, 2017, **29**, 1703063.
- 3 K. A. Peterson, E. M. Thomas and M. L. Chabinyc, *Annu. Rev. Mater. Res.*, 2020, **50**, 551–574.
- 4 D. T. Scholes, S. A. Hawks, P. Y. Yee, H. Wu, J. R. Lindemuth, S. H. Tolbert and B. J. Schwartz, *J. Phys. Chem. Lett.*, 2015, **6**, 4786–4793.
- 5 L. Müller, D. Nanova, T. Glaser, S. Beck, A. Pucci, A. K. Kast, R. R. Schröder, E. Mankel, P. Pingel, D. Neher, W. Kowalsky and R. Lovrincic, *Chem. Mater.*, 2016, **28**, 4432–4439.
- 6 P. Pingel, M. Arvind, L. Kölln, R. Steyrlleuthner, F. Kraffert, J. Behrends, S. Janietz and D. Neher, *Adv. Electron. Mater.*, 2016, **2**, 1600204.
- 7 E. H. Suh, J. G. Oh, J. Jung, S. H. Noh, T. S. Lee and J. Jang, *Adv. Energy Mater.*, 2020, **10**, 2002521.
- 8 A. E. Mansour, D. Lungwitz, T. Schultz, M. Arvind, A. M. Valencia, C. Cocchi, A. Opitz, D. Neher and N. Koch, *J. Mater. Chem. C*, 2020, **8**, 2870–2879.
- 9 M. Arvind, C. E. Tait, M. Guerrini, J. Krumland, A. M. Valencia, C. Cocchi, A. E. Mansour, N. Koch, S. Barlow, S. R. Marder, J. Behrends and D. Neher, *J. Phys. Chem. B*, 2020, **124**, 7694–7708.
- 10 B. Yurash, D. X. Cao, V. V. Brus, D. Leifert, M. Wang, A. Dixon, M. Seifrid, A. E. Mansour, D. Lungwitz, T. Liu, P. J. Santiago, K. R. Graham, N. Koch, G. C. Bazan and T.-Q. Nguyen, *Nat. Mater.*, 2019, **18**, 1327–1334.
- 11 T. Ye, J. Wang, W. Chen, Y. Yang and D. He, *ACS Appl. Mater. Interfaces*, 2017, **9**, 17923–17931.
- 12 E. J. Lawrence, V. S. Oganessian, G. G. Wildgoose and A. E. Ashley, *Dalton Trans.*, 2013, **42**, 782–789.
- 13 J. Panidi, A. F. Paterson, D. Khim, Z. Fei, Y. Han, L. Tsetseris, G. Vourlias, P. A. Patsalas, M. Heeney and T. D. Anthopoulos, *Adv. Sci.*, 2017, **5**, 1700290.
- 14 R. J. Kwaan, C. J. Harlan and J. R. Norton, *Organometallics*, 2001, **20**, 3818–3820.
- 15 T. Beringhelli, D. Maggioni and G. D'Alfonso, *Organometallics*, 2001, **20**, 4927–4938.
- 16 P. S. Marqués, G. Londi, B. Yurash, T.-Q. Nguyen, S. Barlow, S. R. Marder and D. Beljonne, *Chem. Sci.*, 2021, **12**, 7012–7022.
- 17 G. C. Welch and G. C. Bazan, *J. Am. Chem. Soc.*, 2011, **133**, 4632–4644.
- 18 B. Yurash, D. Leifert, G. N. M. Reddy, D. X. Cao, S. Bibberger, V. V. Brus, M. Seifrid, P. J. Santiago, A. Köhler, B. F. Chmelka, G. C. Bazan and T.-Q. Nguyen, *Chem. Mater.*, 2019, **31**, 6715–6725.
- 19 Y. Han, G. Barnes, Y.-H. Lin, J. Martin, M. Al-Hashimi, S. Y. AlQaradawi, T. D. Anthopoulos and M. Heeney, *Chem. Mater.*, 2016, **28**, 8016–8024.
- 20 M. F. Roberts and S. A. Jenekhe, *Chem. Mater.*, 1993, **5**, 1744–1754.
- 21 J. T. Henthorn and T. Agapie, *Angew. Chem. Int. Ed.*, 2014, **53**, 12893–12896.
- 22 L. L. Liu and D. W. Stephan, *Chem. Soc. Rev.*, 2019, **48**, 3454–3463.
- 23 L. L. Liu, L. L. Cao, Y. Shao and D. W. Stephan, *J. Am. Chem. Soc.*, 2017, **139**, 10062–10071.

- 24 X. Tao, C. G. Daniliuc, R. Knitsch, M. R. Hansen, H. Eckert, M. Lübbesmeyer, A. Studer, G. Kehr and G. Erker, *Chem. Sci.*, 2018, **9**, 8011–8018.
- 25 M.-H. Lee, J.-R. Chen, M. Das, T.-F. Hsieh and C.-M. Shu, *J. Therm. Anal. Calorim.*, 2015, **122**, 1143–1150.
- 26 C. M. Cardona, W. Li, A. E. Kaifer, D. Stockdale and G. C. Bazan, *Adv. Mater.*, 2011, **23**, 2367–2371.
- 27 S. Ko, E. T. Hoke, L. Pandey, S. Hong, R. Mondal, C. Risko, Y. Yi, R. Noriega, M. D. McGehee, J.-L. Brédas, A. Salleo and Z. Bao, *J. Am. Chem. Soc.*, 2012, **134**, 5222–5232.
- 28 F. C. Spano, *J. Chem. Phys.*, 2005, **122**, 234701.
- 29 M. J. Nowak, D. Spiegel, S. Hotta, A. J. Heeger and P. A. Pincus, *Macromolecules*, 1989, **22**, 2917–2926.
- 30 E. Lim, A. M. Glaudell, R. Miller and M. L. Chabinyc, *Adv. Electron. Mater.*, 2019, **5**, 1800915.
- 31 P. Y. Yee, D. T. Scholes, B. J. Schwartz and S. H. Tolbert, *J. Phys. Chem. Lett.*, 2019, **10**, 4929–4934.
- 32 R. Ghosh, A. R. Chew, J. Onorato, V. Pakhnyuk, C. K. Luscombe, A. Salleo and F. C. Spano, *J. Phys. Chem. C*, 2018, **122**, 18048–18060.
- 33 H. Bronstein, D. S. Leem, R. Hamilton, P. Woebkenberg, S. King, W. Zhang, R. S. Ashraf, M. Heeney, T. D. Anthopoulos, J. de Mello and I. McCulloch, *Macromolecules*, 2011, **44**, 6649–6652.
- 34 D. Venkateshvaran, M. Nikolka, A. Sadhanala, V. Lemaury, M. Zelazny, M. Kepa, M. Hurlhangee, A. J. Kronemeijer, V. Pecunia, I. Nasrallah, I. Romanov, K. Broch, I. McCulloch, D. Emin, Y. Olivier, J. Cornil, D. Beljonne and H. Sirringhaus, *Nature*, 2014, **515**, 384–388.
- 35 A. I. Hofmann, R. Kroon, S. Zokaie, E. Järsvall, C. Malacrida, S. Ludwigs, T. Biskup and C. Müller, *Adv. Electron. Mater.*, 2020, **6**, 2000249.
- 36 J. Hwang and A. Kahn, *J. Appl. Phys.*, 2005, **97**, 103705.
- 37 J. Hynynen, D. Kiefer and C. Müller, *RSC Adv.*, 2018, **8**, 1593–1599.
- 38 D. T. Scholes, P. Y. Yee, J. R. Lindemuth, H. Kang, J. Onorato, R. Ghosh, C. K. Luscombe, F. C. Spano, S. H. Tolbert and B. J. Schwartz, *Adv. Funct. Mater.*, 2017, **27**, 1702654.
- 39 E. M. Thomas, K. A. Peterson, A. H. Balzer, D. Rawlings, N. Stingelin, R. A. Segalman and M. L. Chabinyc, *Adv. Electron. Mater.*, 2020, **6**, 2000595.
- 40 C. Enengl, S. Enengl, S. Pluczyk, M. Havlicek, M. Lapkowski, H. Neugebauer and E. Ehrenfreund, *ChemPhysChem*, 2016, **17**, 3836–3844.
- 41 M. B. Qarai, R. Ghosh and F. C. Spano, *J. Phys. Chem. C*, 2021, **125**, 24487–24497.
- 42 I. Zozoulenko, A. Singh, S. K. Singh, V. Gueskine, X. Crispin and M. Berggren, *ACS Appl. Polym. Mater.*, 2019, **1**, 83–94.
- 43 D. Neusser, C. Malacrida, M. Kern, Y. M. Gross, J. van Slageren and S. Ludwigs, *Chem. Mater.*, 2020, **32**, 6003–6013.
- 44 K. Kaneto, Y. Kohno and K. Yoshino, *Mol. Cryst. Liq. Cryst.*, 1985, **118**, 217–220.
- 45 Z. Liang, H. H. Choi, X. Luo, T. Liu, A. Abtahi, U. S. Ramasamy, J. A. Hitron, K. N. Baustert, J. L. Hempel, A. M. Boehm, A. Ansary, D. R. Strachan, J. Mei, C. Risko, V. Podzorov and K. R. Graham, *Nat. Mater.*, 2021, **20**, 518–524.
- 46 T. J. Aubry, K. J. Winchell, C. Z. Salamat, V. M. Basile, J. R. Lindemuth, J. M. Stauber, J. C. Axtell, R. M. Kubena, M. D. Phan, M. J. Bird, A. M. Spokoyny, S. H. Tolbert and B. J. Schwartz, *Adv. Funct. Mater.*, 2020, **30**, 2001800.

- 47 M. G. Voss, D. T. Scholes, J. R. Challa and B. J. Schwartz, *Faraday Discuss.*, 2019, **216**, 339–362.
- 48 Y. Xuan, X. Liu, S. Desbief, P. Leclère, M. Fahlman, R. Lazzaroni, M. Berggren, J. Cornil, D. Emin and X. Crispin, *Phys. Rev. B*, 2010, **82**, 115454.
- 49 E. Lim, K. A. Peterson, G. M. Su and M. L. Chabinyc, *Chem. Mater.*, 2018, **30**, 998–1010.
- 50 I. E. Jacobs, E. W. Aasen, J. L. Oliveira, T. N. Fonseca, J. D. Roehling, J. Li, G. Zhang, M. P. Augustine, M. Mascal and A. J. Moulé, *J. Mater. Chem. C*, 2016, **4**, 3454–3466.
- 51 D. T. Duong, C. Wang, E. Antono, M. F. Toney and A. Salleo, *Org. Electron.*, 2013, **14**, 1330–1336.
- 52 T. J. Aubry, J. C. Axtell, V. M. Basile, K. J. Winchell, J. R. Lindemuth, T. M. Porter, J.-Y. Liu, A. N. Alexandrova, C. P. Kubiak, S. H. Tolbert, A. M. Spokoyny and B. J. Schwartz, *Adv. Mater.*, 2019, 1805647.
- 53 L. L. Liu, L. L. Cao, D. Zhu, J. Zhou and D. W. Stephan, *Chem. Commun.*, 2018, **54**, 7431–7434.
- 54 L. L. Cao, K. L. Bamford, L. L. Liu and D. W. Stephan, *Chem. - Eur. J.*, 2018, **24**, 3980–3983.
- 55 A. F. Paterson, L. Tsetseris, R. Li, A. Basu, H. Faber, A.-H. Emwas, J. Panidi, Z. Fei, M. R. Niazi, D. H. Anjum, M. Heeney and T. D. Anthopoulos, *Adv. Mater.*, 2019, **31**, 1900871.